Supplementary Materials for

Structured high-dimensional internal cortical states deduced from fixed tactile input patterns

Johanna Norrlid[1†], Jonas M.D. Enander[1†], Hannes Mogensen[1] and Henrik Jörntell[1]*

Correspondence to: henrik.jorntell@med.lu.se

This PDF file includes:

Material and Methods

Ethics

All animal experiment procedures in the present study were in accordance with institutional guidelines and were approved in advance by the Local Ethics Committee of Lund, Sweden (permit ID M118-13).

Surgical procedures

Adult male Sprague Dawley rats (N=10, weight 240–383 g) were sedated with isoflurane (3%, 1-2 minutes), anesthetized with an intraperitoneal injection (40 mg/kg ketamine, 4 mg/kg xylazine) and maintained under anesthesia with a continuous infusion (ketamine and xylazine in a 20:1 ratio, appx. 5 mg/kg ketamine/hour) administered through an intravenous (IV) catheter inserted into the right femoral vein. A hemicraniectomy (appx 4 by 2 mm) exposed the area of the right somatosensory cortex (Fig. 1B). An ECoG electrode was positioned on the surface of the brain in order to continuously monitor the depth of anesthesia by ensuring the presence of sleep spindles and desynchronized activity, a characteristic of deep sleep (*1*). The level of anesthesia was additionally characterized by an absence of withdrawal reflexes in response to noxious pinches of the hind paw. The type of anesthesia used here has no disruptive effect on the physiological network structure as judged by the preservation of the order of neuronal recruitment of neocortical neurons in spontaneous brain activity fluctuations (up states, recordings obtained using multielectrode arrays in the rat) and stimulus-evoked responses (*2*). Anesthesia drags down the overall activity in the neocortical network (*3*), though, and in general can be expected to make those networks function with a lower degree of precision. Nevertheless, for the present study, the method of stimulus delivery (see below) would not be accepted by the awake animal and meeting the requirement for long term intracellular recordings was further facilitated by the anesthesia. To create further mechanical stability, and to protect the brain tissue from dehydration, an agarose gel was applied to cover the exposed part of the cortex. After finishing the neuronal recordings the animal was sacrificed with pentobarbital (140 mg/kg IV).

Electrical tactile stimulation

Using a bionic fingertip, we previously generated a predefined set of eight spatiotemporal stimulation patterns (*4-7*). The bionic fingertip was moved against different types of objects and the number label of each pattern (Fig. 1A) indicates the radius of the curvature of different objects used to generate each specific pattern, whereas the letter of the label indicates the adaptive tuning of the biomorphic sensors (S, F; for slow and fast, respectively). These spatiotemporal stimulation patterns were delivered via four pairs (or channels) of intracutaneous needle electrodes in a pre-defined random order, where each pattern lasted for less than 340 ms and the consecutive deliveries of the patterns was separated by 1.8 s in order to allow a relaxation of the cortical activity between consecutive deliveries of stimulation patterns (*5*). Each of the eight patterns was delivered 100 times, except for four out of the total thirteen neurons for which the recording was lost after 36, 47, 50 and 80 repetitions, respectively. In addition, for each of the four stimulation channels used, we delivered approximately the same number (up to 100) of repetitions of isolated single pulse stimulations. These isolated single pulse stimulations were delivered in chunks of five stimulations from the same channel separated by 300 ms from each other. Hence, for each channel there was 20 such chunks intermixed with the stimulation patterns in a random order. Each channel was stimulated at 0.5 mA with a pulse width of 0.14

ms, which is higher than the threshold of about 0.2 mA reported for tactile afferents using this type of electrocutaneous stimulation (*8, 9*), but lower than the threshold for activating nociceptive afferents (*10*).

Neural recordings

We made recordings in the region of the S1 cortex of the forepaw, as estimated by the focus of the local field potentials (measured between layers III and V, corresponding to the depths of maximum field potential negativity recorded in each track). The coordinates of this region were -1.0–1.0 mm relative to bregma and 3.0-5.0 mm lateral to the midline (Fig. 1B). Individual neurons were recorded with patch clamp pipettes in the intracellular, whole cell current clamp mode. Patch clamp pipettes were pulled from borosilicate glass capillaries to 6–15 MOhm using a Sutter Instruments (Novato, CA) P-97 horizontal puller. The composition of the electrolyte solution in the patch pipettes was (in mM) potassium-gluconate (135), HEPES (10), KCl (6.0), Mg-ATP (2), EGTA (10). The solution was titrated to 7.35–7.40 using 1 M KOH. During slow advancement of the recording electrode (approximately 0.3 μm per second) made with positive pressure applied, electrode tip resistance and responses evoked by electrical skin stimulation were continuously monitored to identify encounters with neurons. Once encountered, the positive pressure was changed to a negative pressure, and a weak hyperpolarizing current was applied with the aim of obtaining a GigaOhm seal on the neuron. Successful access to the intracellular signal of the neuron, following additional negative pressure once the seal was established, was followed by a release of pressure and the start of the data collection. All intracellular data was digitized at 100 kHz using CED 1401 mk2 hardware and Spike2 software (Cambridge Electronics Devices, CED, Cambridge, UK). The criteria used for inclusion of an intracellular recording, or the time period of such a recording to be included in the analysis, were a stable membrane potential of <-55 mV in down states, a spike amplitude of >25 mV before and after the termination of the protocol and a peak-to-peak difference between the up and down states of >10 mV. All neurons recorded were putatively located within layer III-V based on the recording depth measured from the cortical surface (*11*). For identification of neuron identity, in addition to depth, we used the nature of the firing during spontaneous activity (i.e. if the neuron was fast-spiking, bursting and what duration and intensity of bursts the neuron displayed). All neurons recorded here exhibited infrequent bursts of two or three spikes but had an absence of longer bursts or sustained periods of high firing. Based on this criterion, they were considered to be pyramidal cells rather than interneurons (*12*). Three out of the thirteen successfully recorded neurons were also stained with neurobiotin and histologically recovered. They were thereby confirmed to be pyramidal neurons located in layer III (Fig. 1C).

Post processing - general

The neuronal recording signal was imported from Spike2 to Matlab (2016a, Mathworks), where it was low-pass filtered using a moving average over 50 μs, i.e. 5 samples width given a 100 kHz sampling rate. Stimulation artefacts were removed using a combination of adaptive filtering and blanking of artefacts. Using a weak hyperpolarizing bias current, neurons were prevented from spiking. Occasional remaining intracellular spikes were removed using adaptive filtering, with a recursive fitting algorithm that created a generic spike shape for the neuron (*13*), which could be subtracted from all occurrences of the spike. This allowed for EPSP-like events to be detected also when the membrane potential was influenced by spiking activity. Since all

evoked responses were analysed by visual inspection, there was a quality check of the intracellular signal throughout the recording period.

Post processing – response types

On visual inspection, the time-voltage curves of the intracellular responses to repetitions of a given stimulation pattern appeared to fall into certain types (Fig. 2A), where the differences between responses of different types appeared to be larger than the variability of different responses within any given type.

To quantitatively evaluate the possible existence of specific types of intracellular time-voltage responses to a given stimulation pattern in each given neuron, we used an unsupervised analysis method. Since the number of response types and the number of members of each response type were unknown, the method had to be able to detect zero or more groups of similar response types and it had to be able to identify the number of members for each response type (out of the 100 responses available for each stimulation pattern). Furthermore, the uniqueness of the time voltage curve for each response type had to be evaluated against all other responses as a validation of that the grouping into response types was sound. The following procedure was developed to sort the intracellular responses into types:

1. For each cell, the 350 ms time-voltage curves from the onset of stimulation for each of the 100 repetitions of a given stimulation pattern were compared.
2. To remove high-frequency fluctuations the responses were low-pass filtered (with a 1 ms wide moving average) and re-sampled to 1000 Hz. In order to focus on the temporal shape of the responses, the response voltage were then normalized to a 1.0 - 0.0 range based on the highest peaks and deepest troughs for each 350 ms time-voltage curve. This was made to ensure that the method captured the shape of the response over time.
3. For each neuron/stimulation pattern, each time-voltage curve was compared against all time-voltage curves of that set for pairwise identification of similarity. The similarity evaluation between two time-voltage curves was done on the normalized voltage on a per sample time unit basis, where the difference for each sample point was calculated in turn. The mean difference between the curves was calculated by first calculating the absolute difference. If the difference for a sample point was below a threshold value (this 'Threshold difference' was set to 0.13 normalized units, see Fig. S2), the difference was set to zero for that sample point. If the difference was above the threshold value, the overshoot was calculated as the absolute value of the actual difference above the threshold value. The mean overshoot was calculated as the total sum of the overshoots for all sample points divided by the number of samples (350). If the mean overshoot fell below a threshold (this 'Overshoot threshold' was set to 0.08 normalized units, see Fig. S2) the two time-voltage curves was classified as being of the same response type. This procedure helped reducing sensitivity to high amplitude but transient membrane potential shifts, while preserving the sorting resulting from persistent low amplitude differences between time-voltage curves.
4. This procedure was repeated so that all time-voltage curves were compared with all others of the neuron/stimulation pattern group (i.e. typically 100 responses). This resulted in the identification of several types of responses. The members of the response type with the largest number of members were removed from the set of 100 responses, and the sorting (steps 1 -4) was repeated until there were no remaining responses left to sort.

5. Last, for the set of detected response types, for each response type with less than 5 members, the members were categorized as belonging to the 'ungrouped' response type and that response type was no longer a valid response type.

Selection of parameter values

The method described above is unsupervised, but depend on the choice of parameter values for the Threshold difference and the Overshoot threshold (step 3 above). The Threshold difference parameter is a static voltage distance to the reference response (Fig. 2B, blue area). The Overshoot threshold is also a voltage distance, but is a dynamic threshold instead of a static.

The choice of parameter values was based on the aims to maximize the average classification of the kNN procedure (described below) and to minimize the number of ungrouped responses while still keeping the number of response types reasonable (for most stimulation patterns more than one, but fewer than the total number of raw responses). To test the sensitivity of the method to the choice of parameter values, we explored the resulting outcome across parts of the parameter space for two neurons' sets of responses to different stimulation patterns. This exploration is visualized in Figure S2, which suggested that our choices of parameter values were located in the middle of a smooth landscape of outcomes.

Statistical evaluation of the identified response types

After having grouped the responses into types, we next explored to what extent this response types were different from each other, and how that difference varied as a function of time, both during the unfolding of the stimulation patterns and after the termination of those stimulations. For each time point of the down-sampled data (see above), we took all the responses classified to each type and compared it with the normalized voltage (see above) of all other responses evoked by the same stimulation pattern in the same neuron, using the Kruskal-Wallis test. Hence, for each time point we got a p-value of the probability of observation given H0 that there were no differences between the different response types. This procedure was repeated for each time point up to 1200 ms after the onset of the stimulation pattern. The procedure was repeated for other types in other stimulation patterns in the same neuron until all response types of all stimulation patterns in each neuron had been analysed separately (as displayed in Fig. S3). The fraction of the responses that fell $p<0.05$ limit as a function of time was also analyzed and compared with shuffled data, where the responses were shuffled among the type classes but kept within the same stimulation pattern and the same neuron (Fig. 2C).

Evaluation of the specificity of the identified response types for each stimulation pattern

The separability of the identified response types, as well as the separability versus the 'ungrouped' responses, was further evaluated using a combination of PCA and kNN-classification. As the previous procedure was used to identify possible subtypes of responses within a finite set of intracellular responses to a given stimulation pattern using pairwise comparisons, this procedure was used to compare these response types against all of the responses evoked by the same stimulation pattern.

i. Using the mean signal of each valid response type, we calculated the Principal Components (PCs). The number of PCs used was the number required to explain at least 95% of the total variance of the mean signals. Finally, we used the principal component coefficients to transform each recorded time-voltage curve from the time domain to the principal component domain, reducing the dimensionality of each response from M = 350 to N = [1-6] (PCs).

ii. The classification was performed using the principal component coefficients from the previous step. In order to determine the separability of the detected groups, and the possible confusion in relation to the 'ungrouped' responses, we used a kNN classification procedure. Half of the responses were randomly selected as the training set. For each response belonging to the test set we identified the 4 closest responses in the training set by calculating the Euclidian distance in PC space. The response was classified as belonging to the same response type as the relative majority of the 4 neighbours. We performed 40 iterations of the classification, each with a different training set, and averaged the fraction of correctly classified responses in each iteration to get the mean correct classification value for the response types.

The analysis of the intracellular responses using PCA always included the first 350 ms of the evoked responses unless otherwise indicated. The results of the ensuing kNN decoding are visualized in confusion matrices such as Fig. 2C, which were also used to extract the mean decoding accuracy and the F1 score.

Evaluation of the specificity of the response types across the stimulation patterns

To evaluate if the identified response types were specific to the stimulation pattern, we again used PCA and kNN-classification. Steps i and ii as above were performed as described but across all eight stimulation patterns. As the total number of responses considered was in the order of 800 rather than 100, the dimensionality of the responses was reduced to N = [8-40] PCs, rather than [1-6] PCs as in the above analysis confined to response types within each stimulation pattern. The number of neighbours evaluated for the kNN classification was in both cases nine (N=9). Finally, we also used PCA and kNN decoding to evaluate if the response types were specific to the neuron, for each specific stimulation pattern (see for example Fig. 3D), using the same type of approach as described here.

Post processing - responses evoked by individual stimulation pulses within patterns

We also performed an analysis of the responses to the individual pulses within the different stimulation patterns (Fig. S3-S5). We constrained the analysis to the following set of individual stimulation pulses: Each of the eight spatiotemporal stimulation patterns consisted of 5-33 individual stimulation pulses and a total sum of 152 pulses altogether in the eight patterns used (Fig. 1A). The time between subsequent stimulation pulses within the stimulation patterns varied in the span 1-123 ms. This means that in some cases, the intervals between subsequent stimulation pulses were too short to identify which of the pulses generated the recorded response. Since the scope of this part of the analysis was to investigate the response to specific in-pattern stimulation pulses, only stimulation pulses that were temporally segregated from previous and subsequent pulses by at least 10 ms were included (as the average response latency time was 11 ms, Table S1). Based on this selection criterion, 52 out of the total 152 pulses were included in the analysis of the responses evoked by the individual stimulation pulses within stimulation patterns.

Responses to the individual stimulation pulses were analysed both manually and automatically. The manual part of the analysis consisted in a visually guided definition of the onset latency, amplitude height and latency-to-peak using a tailor-made point-and-click user interface (as in Fig. 1E-G). The automatic part consisted of a detection of EPSP-like events using tailored template matching routines – its sole purpose was to identify if EPSPs evoked by a particular stimulation pulse were so infrequent that they were at risk of not surpassing the

spontaneous occurrence of similar EPSP events (in the recording times in between the presentation of the stimulation patterns), in which case they were to be excluded from further analysis. EPSP templates consisted of a series of 5-20 time-voltage thresholds with individually variable voltage variance and were defined manually for each neuron based on a large sample of EPSP-like events (>>100) occurring after in-pattern stimulation pulses. They were visually confirmed to not omit mid to large EPSP-like events (> 3 mV) that occurred spontaneously at randomly sampled time points throughout the duration of the recordings. The response fraction of a neuron to each repetition of a stimulation pulse was defined as the number of repetitions evoking an EPSP-like event, as judged by the automated EPSP identification in the time range 4 - 18 ms after the pulse onset, divided by the total number of repetitions of that pulse. The baseline activity of that same EPSP-like event was determined by counting its spontaneous activity in time bins of 14 ms width (i.e. the same width as the response window) for 12 consecutive bins preceding the onset of the stimulation pattern. As each stimulation pattern as a rule was repeated 100 ms, we typically obtained a total of 1200 such bins. The response fraction of the spontaneous activity was obtained by taking the average activity across these 1200 bins. The threshold activity for the EPSP template, i.e. the response fraction that an in-pattern stimulation pulse needed to exceed in order to qualify as an evoked rather than spontaneous response, was defined as the mean plus two standard deviations of the response fraction of the spontaneous activity. If the response fraction was below the threshold activity, or if there was less than five manually detected EPSPs, the response of that in-pattern stimulation pulse was considered not significant and was discarded from further analysis.

Brain state segmentation

During each neuronal recording, a parallel ECoG signal was recorded at a sample rate of 1 kHz from the surface electrode placed on the surface of the cortex (Fig. 1B). To segment the recording into epochs occurring under synchronized versus desynchronized ECoG states, the spectral density of the ECoG was calculated with a segment length of 1,000 ms, an overlap of 125 ms and a constant (mean) detrending. The spectral density of Delta, Theta and Alpha bands (0–12 Hz) was summed for each segment and the compound value was used for the remainder of the analysis. A desynchronized segment of ECoG was assumed to occur when the compound spectral density dropped below the compound spectral density median for at least two segments in sequence. For each recording, every stimulus presentation, and thereby also each response state, was classified as occurring either during an asynchronous or a synchronous brain state based on which state the ECoG signal was at the onset of the stimulation. The fraction of stimulus presentations that occurred within the desynchronized state relative to the total number of presentations was used for statistical comparisons (Fig. S7). As the probability of a brain state is expected to influence the observed ratios of occurrences of events within each brain state the statistical method used to make the comparisons was the paired t-test.

Statistical analysis

For pairwise comparisons of EPSP-like responses (Fig. S1, S5-S6), we used the Wilcoxon rank sum test for pairwise comparisons as the data was not obviously following a normal distribution. For statistical evaluation of the identified response types, we used the Kruskal-Wallis test (Fig. 2C; Fig. S3). For pairwise tests of response fractions occurring under desynchronized brain states (Fig. S7), we used paired t-test.

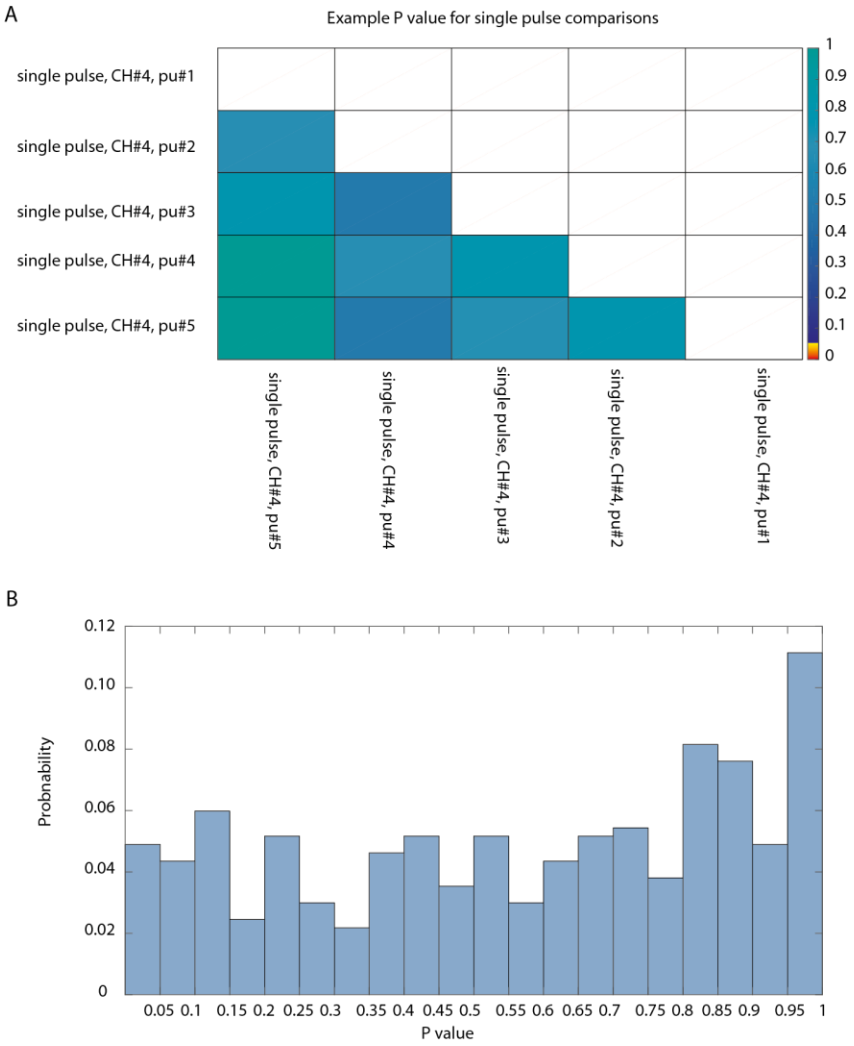

Fig. S1. The variability of the isolated single pulse responses was independent of the order in which they appeared. Each isolated single pulse stimulation per channel occurred in chunks of five repetitions separated from each other by 0.3 s, whereas different chunks of stimulation were randomly intermixed with the full stimulation patterns. Here, we analyzed if the variability of the isolated single pulse responses were dependent on the order in which they appeared within chunks. (**A**) Illustration of the statistical test used for a sample stimulation channel in a sample neuron. For each stimulation channel, there were 10 comparisons that could be made. In this case, none of the 10 comparisons resulted in any statistically significant difference in the response amplitude (Wilcoxon rank sum test for pairwise comparisons, p-values are indicated according to the color scale). Hence, the amplitude of the responses to isolated single pulse stimulation was not affected by the order of presentation within chunks at the 0.3 s intervals used. (**B**) The distribution of p-values across all neurons and all stimulation channels (binned) suggested a chance distribution. Hence, also across the population as a whole, we could not find any order-dependence of the amplitudes for the responses evoked by the isolated single pulse stimulations.

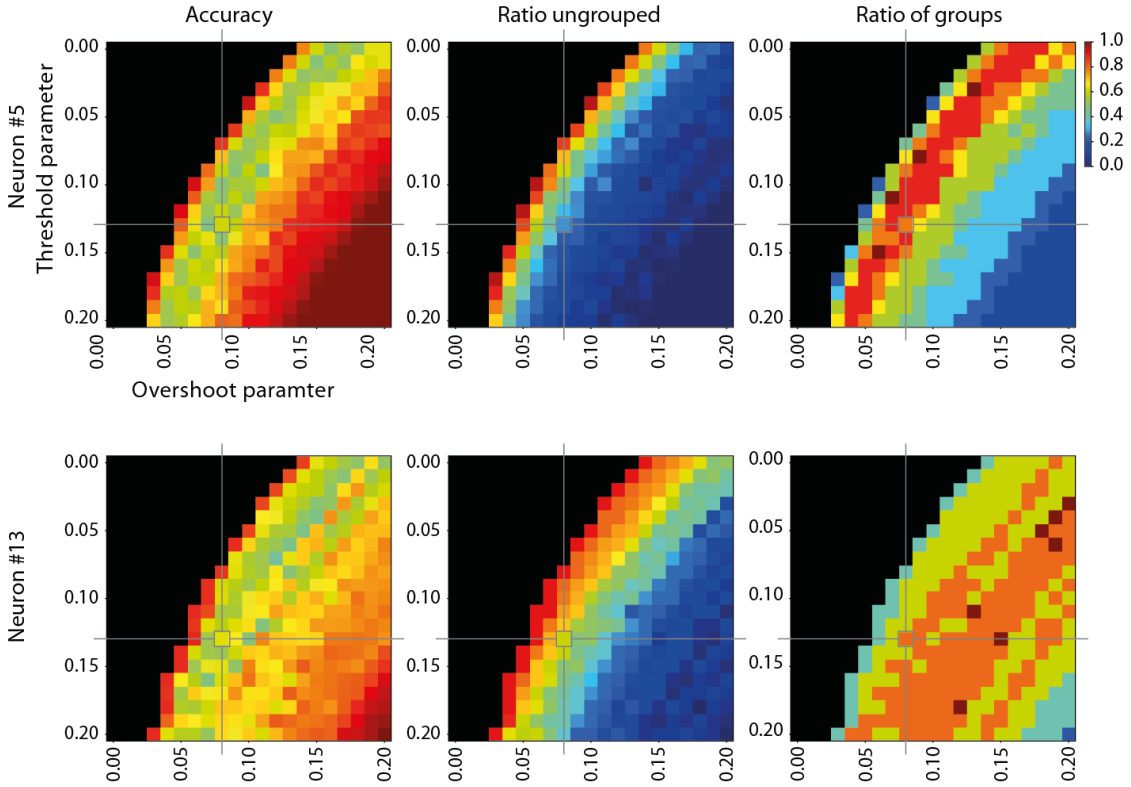

Fig. S2. **Sensitivity analysis of the parameter choice in the response type identification method.** We explored the resulting outcome across parts of the parameter space for two neurons' sets of responses to different stimulation patterns. This exploration indicates that the choice of parameter values (crosshair) for the 'Threshold parameter' and the 'Overshoot parameter' (see Methods) were located in the middle of a smooth landscape of outcomes. It also shows that the choice of parameter values resulted in a balance between decoding accuracy (see Fig. 2C), the ratio of ungrouped versus the responses that were type classified, and the number of response types identified normalized to the maximal number found for that neuron.

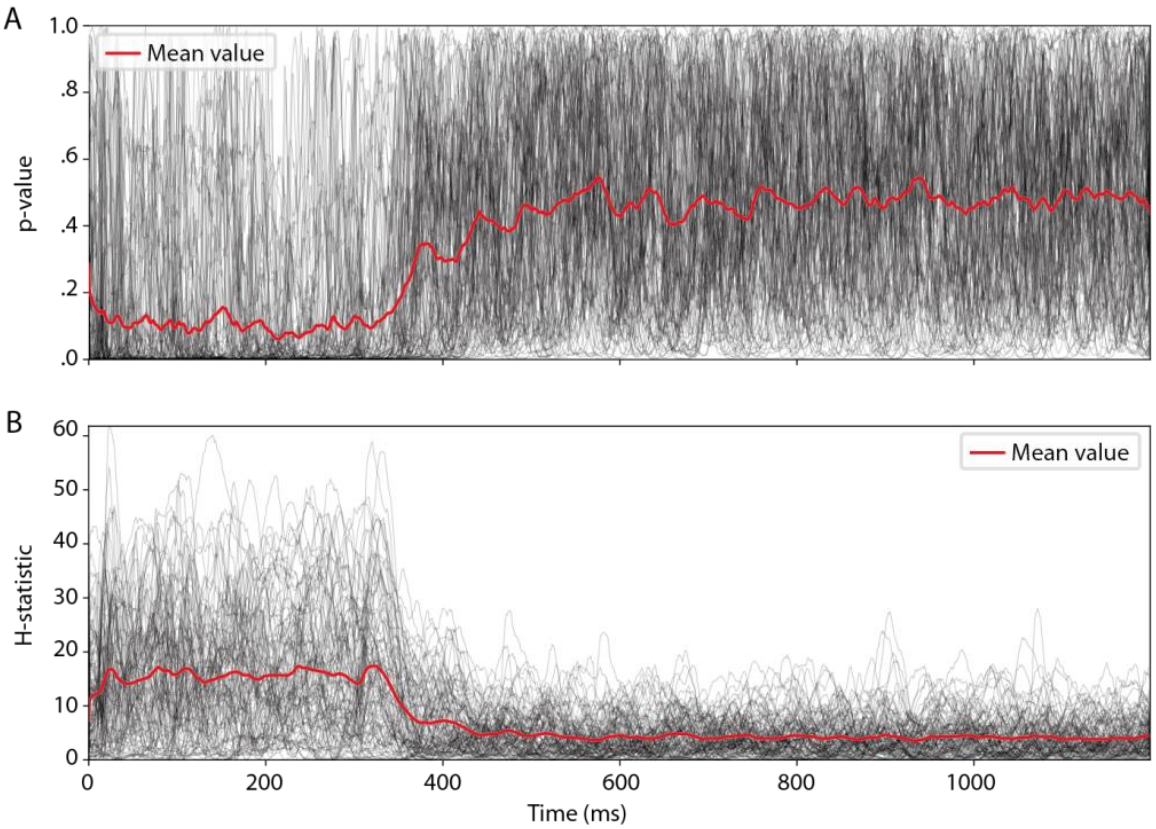

Fig. S3. Specificity of response type separation varied over time

(A) The Kruskal Wallis result of the separation between the responses of one response type from all the other responses evoked by same stimulation pattern in the same neuron, plotted for each identified response type (N=494) for every sample time point (for data downsampled to 1000 Hz) in grey traces. The red trace represents the average of all curves. (B) Corresponding plot for the H statistic.

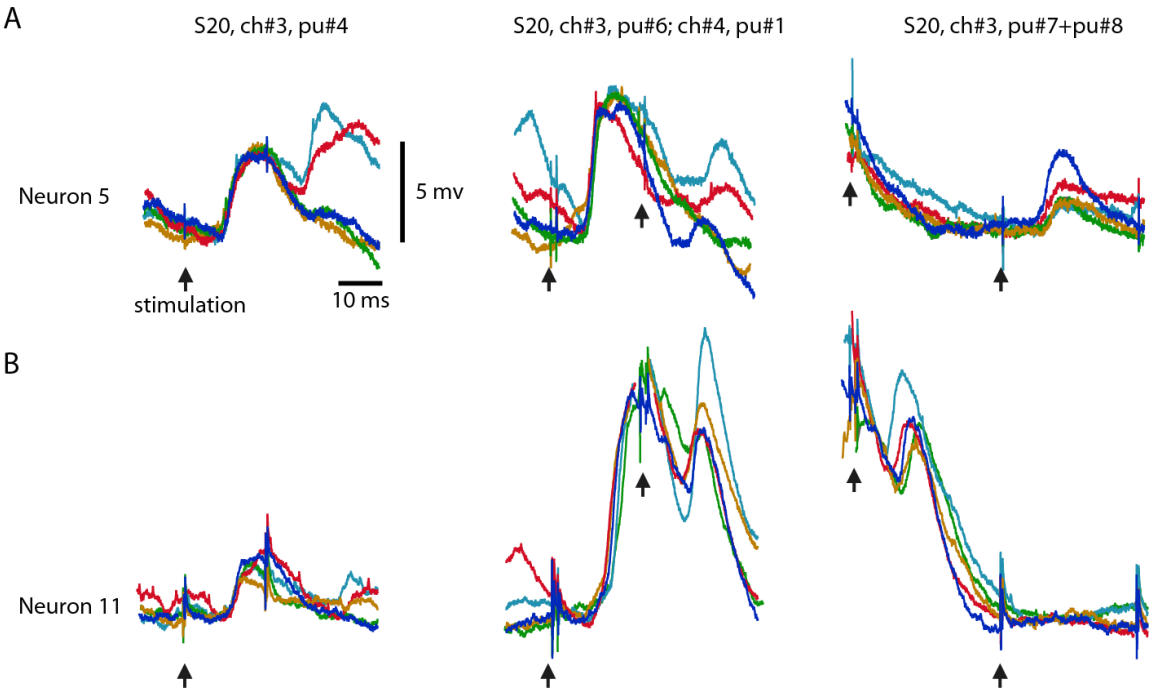

Fig. S4. Intracellular raw data responses to single pulse stimulation of the same channel varied with position in the stimulation pattern. (**A**) Five superimposed raw data traces for the responses of neuron#5 to stimulation of ch#3 in various positions (as indicated by pu# and arrows below traces) within stimulation pattern S20. (**B**) Similar display for neuron#11.

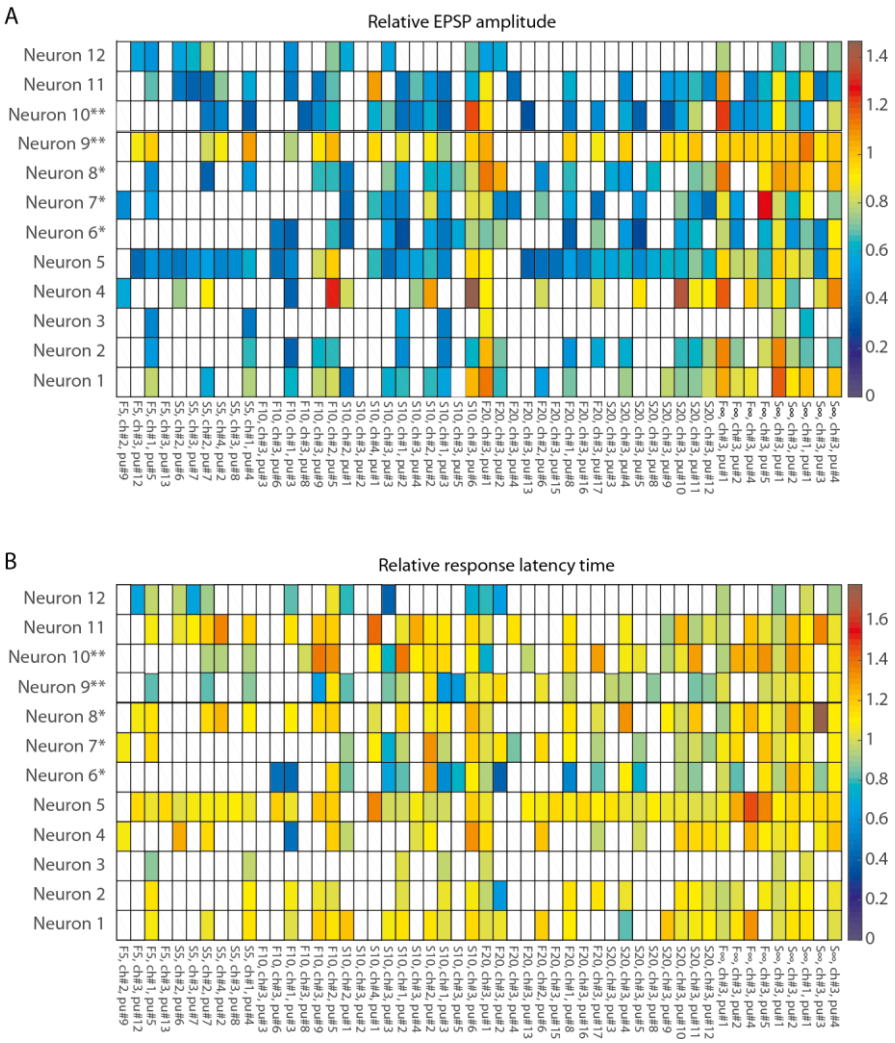

Fig. S5. Relative changes in response amplitude and latency time depending on position within stimulation patterns across all neurons and stimulation pulses. (A) Average EPSP amplitude, indicated as multiples of the average EPSP amplitude to the isolated single pulse stimulation of the corresponding channel (Fig. 1E), for each neuron and each analyzed within-pattern stimulation pulse (N=52), corresponding to an analysis of a total of 56762 responses to isolated single pulse stimulations. Neuron ID is given to the left, where asterisk symbols are used to indicate neurons recorded from the same experiments. For each analyzed stimulation pulse, the stimulus pattern and the sequential position of the pulse within that pattern (pu#) for each respective stimulation channel (ch#) are indicated at the bottom (organized according to their order of occurrence within the stimulation patterns). White entries indicate that the response fraction did not surpass the spontaneous level of EPSP events by more than two standard deviations according to the automatic EPSP detection method and the response was hence discarded from further analysis. (**B**) Similar display as in **A**, but for the relative response latency time, i.e. the latency expressed as multiples of the average response latency time to isolated single pulse stimulation of the corresponding channel. Altogether, these results (**A**-**B**) is in line with the outcome of the response type identification analysis above by illustrating that those findings cannot be explained by assuming a generic sequence of paired-pulse depression or facilitation phenomena that would affect all neurons in the same way.

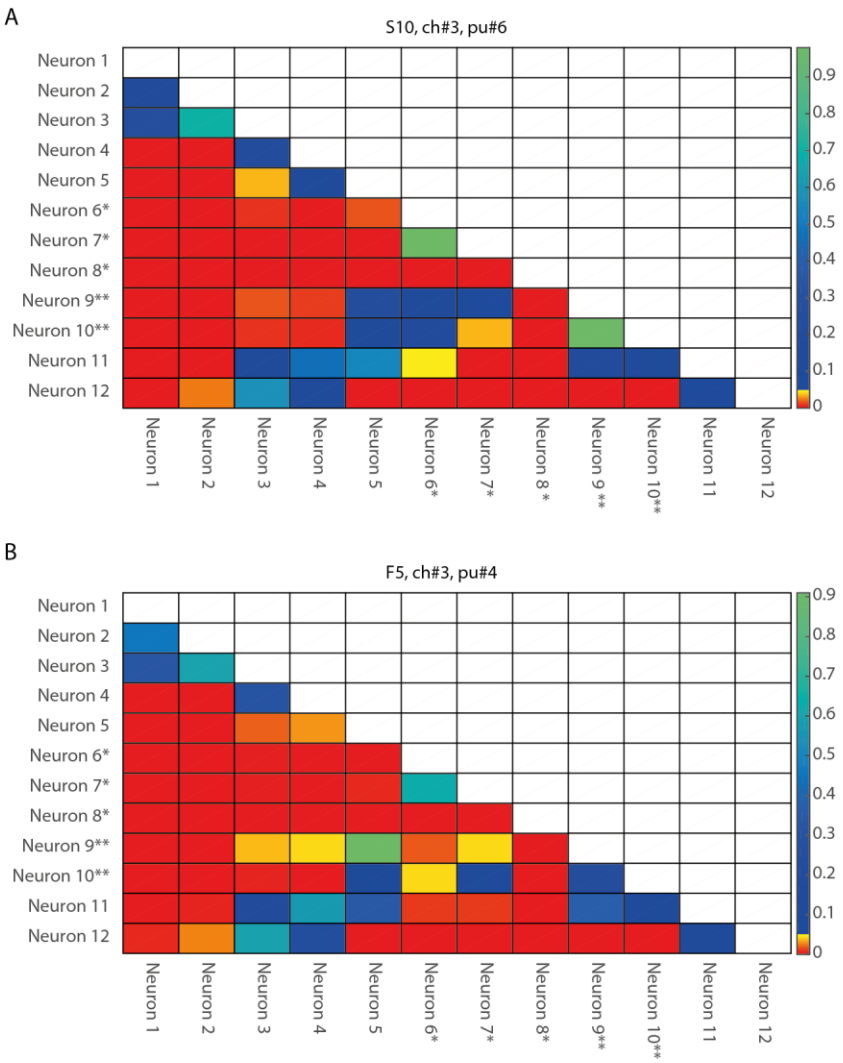

Fig. S6. Pairwise comparisons of differences in EPSP metrics. (**A-B**) For two sample stimulation pulse positions (S10, ch#3, pu#6; F5, ch#3, pu#4 we analyzed whether the changes in relative EPSP amplitude (compared to the neuron's isolated single pulse response) differed between neurons. The p-values of the Wilcoxon rank sum test for pairwise comparisons of the raw EPSP-like responses are reported as a color code in the matrix where all 12 neurons were compared (N=56 comparisons).

When the same analysis was performed across all 52 stimulation pulse positions (see Fig. S4) statistically significant differences between the neurons (at $p<0.05$, Wilcoxon rank sum test for pairwise comparisons; the analysis only included responses that were non-white entries, i.e. statistically significant, in Fig. S5) were found in 65 % of the comparisons of the amplitudes, 78% of the comparisons of the times-to-peaks and 86% of the comparisons of the response latency times. Hence, for the majority of the in-pattern stimulation pulses, the changes in response amplitude, time to peak and latency relative to the isolated single pulse stimulation were statistically different between the neurons, corroborating the results from Figs 2 and 3 that each neuron exhibited partly unique sequences of response modulations across the duration of the stimulation patterns.

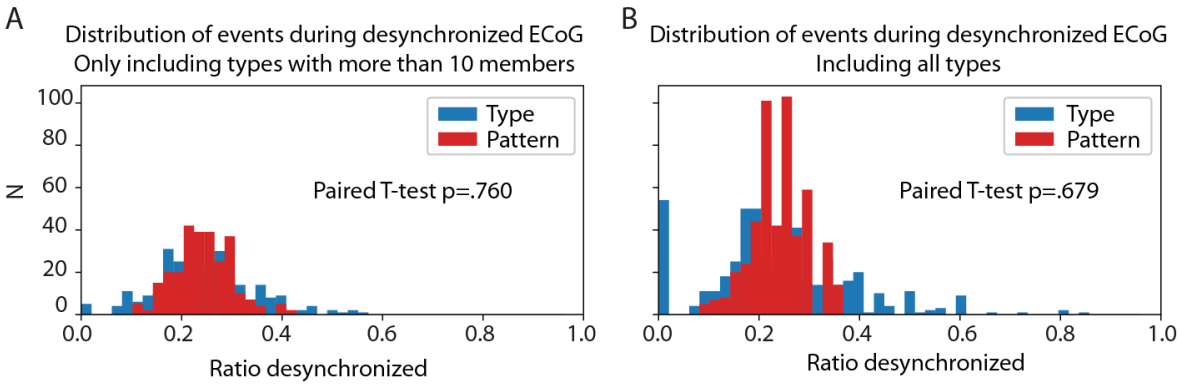

Fig. S7. Incidence of specific response types versus ECoG state. The fraction of responses generated in the desynchronized ECoG state for all responses evoked by each stimulation pattern in each neuron (red) and for each response categorized by response type (blue). The fraction for each response type is hence paired with the corresponding fraction for the stimulation pattern. (**A**) The bar chart illustrates the results of this investigation only for response types with more than nine members (nine responses). (**B**) Same display but for all response types identified. Note that the peak at 0.0 and several very high values for the type-separated responses (blue bars) depended on that some response types had only 5-9 members. As the overall probability of being in the desynchronized ECoG state was around 20%, chance omission or addition of one response in the desynchronized state was very likely, and this could explain these outlier bars. Nevertheless, under both circumstances (**A-B**) the response types were not distributed significantly differently from the overall responses evoked by the same stimulation pattern according to the paired t-test.

MEAN +/- STD	Peak amplitude	Response onset latency time	Latency to peak
CV	0.43+/-0.10	0.28+/-0.10	0.29+/-0.08
Values	7.7+/-4.8 mV	11.1+/-3.1 ms	9.8+/-5.6 ms

Table S1. Quantification of single pulse responses in the population of neurons. We quantified the response variability across the entire population of neurons using the coefficient of variation (CV) measure. We investigated responses to input from 4 channels for 12 neurons, and hence calculated the CV for N=48 stimulus presentations, each repeated 100 times, as a rule, with 4 exceptions (see Methods). For the CV of the response onset latency time we subtracted a fixed 4 ms delay for the cuneo-thalamo-cortical pathway. The corresponding values are displayed on the second row. Altogether, the data indicated that the three measured response parameters had a large internal variability.

References

1. E. Niedermeyer, F. H. L. da Silva, *Electroencephalography: basic principles, clinical applications, and related fields*. (Lippincott Williams & Wilkins, 2005).
2. A. Luczak, P. Bartho, Consistent sequential activity across diverse forms of UP states under ketamine anesthesia. *The European journal of neuroscience* **36**, 2830 (Sep, 2012).
3. C. M. Constantinople, R. M. Bruno, Effects and mechanisms of wakefulness on local cortical networks. *Neuron* **69**, 1061 (Mar 24, 2011).
4. C. Genna *et al.*, Bilateral tactile input patterns decoded at comparable levels but different time scales in neocortical neurons. *The Journal of neuroscience : the official journal of the Society for Neuroscience*, (Mar 14, 2018).
5. C. M. Oddo *et al.*, Artificial spatiotemporal touch inputs reveal complementary decoding in neocortical neurons. *Scientific reports* **8**, 45898 (Apr 04, 2017).
6. J. M. D. Enander *et al.*, Ubiquitous Neocortical Decoding of Tactile Input Patterns. *Frontiers in cellular neuroscience* **13**, 140 (2019).
7. J. M. D. Enander, H. Jorntell, Somatosensory Cortical Neurons Decode Tactile Input Patterns and Location from Both Dominant and Non-dominant Digits. *Cell reports* **26**, 3551 (Mar 26, 2019).
8. D. D. Rasmusson, S. A. Northgrave, Reorganization of the raccoon cuneate nucleus after peripheral denervation. *Journal of neurophysiology* **78**, 2924 (Dec, 1997).
9. F. Bengtsson, R. Brasselet, R. S. Johansson, A. Arleo, H. Jorntell, Integration of sensory quanta in cuneate nucleus neurons in vivo. *PloS one* **8**, e56630 (2013).
10. C. F. Ekerot, P. Gustavsson, O. Oscarsson, J. Schouenborg, Climbing fibres projecting to cat cerebellar anterior lobe activated by cutaneous A and C fibres. *Journal of Physiology (London)* **386**, 529 (1987).
11. R. T. Narayanan, D. Udvary, M. Oberlaender, Cell Type-Specific Structural Organization of the Six Layers in Rat Barrel Cortex. *Frontiers in neuroanatomy* **11**, 91 (2017).
12. A. Luczak, P. Bartho, K. D. Harris, Spontaneous events outline the realm of possible sensory responses in neocortical populations. *Neuron* **62**, 413 (May 14, 2009).
13. H. Mogensen, J. Norrlid, J. M. D. Enander, A. Wahlbom, H. Jorntell, Absence of Repetitive Correlation Patterns Between Pairs of Adjacent Neocortical Neurons in vivo. *Frontiers in neural circuits* **13**, 48 (2019).